Materials & Design 209 (2021) 110002

Contents lists available at ScienceDirect

Materials & Design

journal homepage: www.elsevier.com/locate/matdes

The effect of the graded bilayer design on the strain depth profiles and microstructure of Cu/W nano-multilayers

A.V. Druzhinin [a,b,c], G. Lorenzin [b], D. Ariosa [d], S. Siol [b], B.B. Straumal [a,c], J. Janczak-Rusch [b], L.P.H. Jeurgens [b], C. Cancellieri [b,*]

[a] National University of Science and Technology «MISIS», Leninskiy Prospect 4, Moscow 119049, Russian Federation
[b] Empa, Swiss Federal Laboratories for Materials Science and Technology, Laboratory for Joining Technologies and Corrosion, Überlandstrasse 129, Dübendorf CH-8600, Switzerland
[c] Institute of Solid State Physics and Chernogolovka Scientific Center, Russian Academy of Sciences, Moscow District, Academician Ossipyan Str., Chernogolovka 142432, Russian Federation
[d] Instituto de Física, Facultad de Ingeniería, Universidad de la República, Herrera y Reissig 565, C.C. 30, Montevideo 11000, Uruguay

HIGHLIGHTS

- The average stress is not representative of the real stress state in nano-multilayer.
- Strain depth profiles are derived and can be tailored by the Cu/W bilayers position.
- Design of the bilayer blocks arrangement is a tool to tailor the Cu surface outflow.
- In homogeneous nanocomposites are formed by thermal degradation of graded multilayers.

GRAPHICAL ABSTRACT

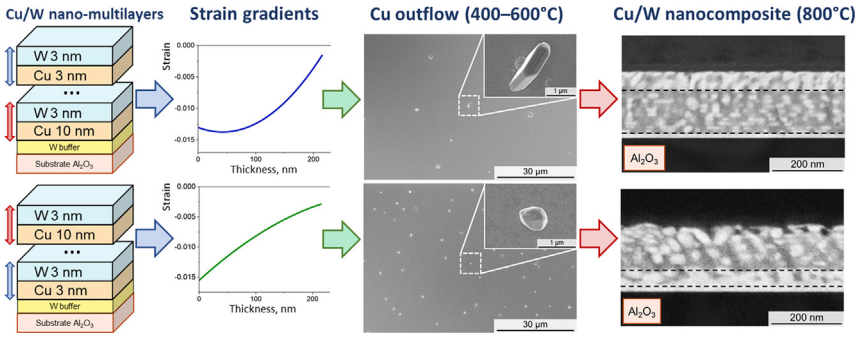

ARTICLE INFO

Article history:
Received 30 April 2021
Revised 14 July 2021
Accepted 22 July 2021
Available online 23 July 2021

Keywords:
Nano-multilayers
Microstructure
Residual stress
Strain gradient
Nanocomposite

ABSTRACT

The properties and thermal stability of thin films and nano-multilayers (NMLs) are generally governed by the in-depth stress (strain) gradients rather than the average stress state. The effect of strain gradient variation in Cu/W NMLs on the thermal stability between 400 and 800 °C was investigated. The strain distribution in the NML stacks was varied by combining Cu/W bilayers with different Cu and W thicknesses of either 3 or 10 nm. A recently developed method based on in-plane grazing X-ray diffraction was adopted to extract the strain depth profiles. In addition, the evolution of the average stress in the Cu/W NMLs during growth was monitored by an *in-situ* wafer curvature technique. The mean residual stresses in Cu and W were found to be independent of the disposition of the different Cu/W bilayer substacks. On the contrary, the strain depth profile of the W nanolayers was found to strongly depend on the disposition of Cu/W bilayer substacks in the Cu/W NML, which resulted in different Cu outflow characteristics upon annealing. Moreover, application of different Cu/W bilayer units within the NML stack also provides an innovative pathway for producing Cu/W nanocomposites with graded thermal and mechanical properties.

* Corresponding author.
E-mail address: claudia.cancellieri@empa.ch (C. Cancellieri).

https://doi.org/10.1016/j.matdes.2021.110002
0264-1275/

1. Introduction

Nano-multilayers (NMLs) are functional architectures which combine nanometer size layers, whose physical properties can be tailored by smart microstructural and interfacial design [1]. These nanomaterials are of great scientific and technological interest, since their nanolaminated architecture offers very flexible design criteria to achieve a unique combination of optical [2,3], magnetic [4,5], mechanical properties [6–8], thermal and electronic conductivity for microelectronic devices [9] and radiation tolerance [10]. For example, specific NML designs with patterned metallic surface nanostructures can be established by variation of the growth parameters, followed by a selected sequence of post-growth treatments, such as thermal annealing [11–14] in combination with a laser treatment [15] or mechanical nano-indentation [16] of the NML surface. As-deposited NML systems typically exhibit a metastable state due to the intrinsically high density of internal interfaces (i.e. grain and phase boundaries associated with an excess Gibbs energy) [17], high residual stresses [14] and non-equilibrium defect concentrations [18].

In particular, residual stresses play one of the major roles in determining mechanical instabilities, failure and reliability issues of these nanomaterials [19]. The main scientific challenge here is that the residual stress distribution is normally not homogeneous across the NML depth (e.g. Ref. [20]), so the stress (strain) gradients dominantly control the functional properties and ultimate performance of NMLs in applications. Intrinsic sources of the residual stress gradients in thin films include those due to the system's microstructure, or those originating from defects during film deposition, self-organization phenomena during grain-growth and post deposition treatments [21]. Thermal energy by e.g. high-temperature annealing can add extrinsic sources of stress associated with thermal expansion mismatch between constituent materials. The microstructural evolution towards a bulk thermodynamic equilibrium state triggered kinetically by e.g. high-temperature annealing is governed by the relaxation of the non-uniform strain distribution. Adjusting the initial NML microstructure in order to control the stress depth distribution is one of the key challenges for achieving a stable microstructure with the desired functional properties.

Among the metallic NMLs, due to the high mechanical strength [22] and fracture toughness [23], radiation tolerance [24,25], combined with the excellent thermal conductivity [9], Cu/W NMLs received a lot of attention in industrial applications [26,27]. In particular, the microstructural transformations upon thermal annealing have been intensively studied for immiscible Cu/W NMLs [14,28–30]. To this end, a high-temperature annealing step is performed to transform the Cu/W NML into a functional nanocomposite (NC) [14,28,29]. The temperature range of the NML-to-NC transformation varies from 700 to 800 °C, depending on the compressive in-plane residual stresses and defect structure [14,30,31]. The NML-to-NC transformation is preceded by the outflow of Cu to the NML surface and subsequent thermal grooving of W/W grain boundaries [28]. The thermal grooving of grain boundaries is a typical mechanism of degradation of the nanolaminated architecture, as also observed for e.g. Cu/Mo [32], Ag/Ni [17,33], Ag/Fe [34], Cu/Co [34,35], Cu/Nb [36], Cu/Ag [37] NML systems. The directional outflow of Cu to the NML surface at the onset of the NML-to-NC transformation (in the temperature range of 400–600 °C) partially relaxes the large residual compressive stresses in the as-deposited Cu/W NML, creating a discrete pattern of Cu nanocrystals on the surface [14,28,30,38].

By changing the individual nanolayer thicknesses, it was shown that the Cu outflow correlates with the magnitude of the mean residual stresses in nanolayers in the as-deposited state, which can be varied [14]. However, the microstructural evolution in Cu/W NMLs could only be correlated to the *mean* values of the residual stresses in the Cu and W nanolayers during different stages of annealing. Evidently, the NML-to-NC transformation and, particularly, the directional surface outflow of Cu, will depend on the *distribution* of stresses (or elastic strains) in the NML volume (i.e. on the stress gradients) rather than on the averaged magnitude of the residual stress. In general, the stress measurement in NMLs is done on an average scale, without taking into account the variation through the depth of the NML. Although the presence of non-uniform strain gradients in single and multiple microlayers is known to exist (e.g. in Cu/W multilayers [39]), its assessment and measurements in the nanometer size systems represent a difficult task. The influence of multilayer design on residual stress gradients has only been reported for micrometer scale multilayers [40].

In the present study, Cu/W NMLs with specific graded bilayer structure consisted of Cu and W nanolayers with different thicknesses are designed in order to tailor the residual stress (strain) distribution. To our knowledge, for the first time, the in-depth strain gradient (strain depth distribution) in Cu/W multilayers with nanometer-scaled layers is measured and its effect on the NML-to-NC transformation is reported. The stress/strain state in deposited Cu/W NMLs is comprehensively studied by a combined experimental-modelling approach. The average strain distribution in the confined W nanolayers across the depth of the Cu/W NML is experimentally resolved by modelling experimental strain depth profiles as measured by in-plane X-ray diffraction (XRD). The corresponding average residual stresses in the Cu and W nanolayers are also derived *ex situ* by from conventional out-of-plane XRD. In addition, the evolution of the average residual stress in the Cu/W NMLs during the deposition process is monitored *in situ* from the change in substrate curvature. The differences in the NML microstructural evolutions upon high-temperature annealing could thus be related to the different strain distributions. The study elucidates how the strain depth distribution in Cu/W NMLs can be varied to tailor the amount of Cu surface outflow as exploited for e.g. joining applications [27]. On the other hand, it is shown that the thermal degradation of Cu/W NMLs with a graded bilayer design can be considered as the novel technique for producing Cu/W NCs with a graded bulk microstructure and *ad-hoc* mechanical and thermal expansion properties. The proposed graded structure design of Cu/W NMLs and the presented method for the derivation of the strain gradient allows the design and fabrication of functional NMLs and NCs for industrial applications.

2. Experimental methods

2.1. Sample preparation

Cu/W NMLs were deposited at room temperature on $10 \times 10\ mm^2$ polished α-Al_2O_3 (0001) single-crystalline wafer substrates (i.e. sapphire-C wafers) of 500 and 330 μm thickness by magnetron sputtering (MS) in an ultrahigh vacuum chamber (base pressure < 10^{-8} mbar) from two confocally arranged, unbalanced magnetrons equipped with targets of pure W (99.95%) and pure Cu (99.99%). Before insertion in the sputter chamber, the sapphire substrates were ultrasonically cleaned using acetone and ethanol. Prior to deposition, possible surface contamination on the α-Al_2O_3 (0 0 0 1) substrate was removed by Ar+ sputter cleaning for 5 min applying an RF Bias of 100 V at a working pressure of 1.6×10^{-2} mbar. NML deposition was carried out at a working pressure of 5×10^{-3} mbar. First, a 25 nm thick W buffer layer was deposited on the sputter-cleaned substrate. Next, Cu/W NML

configurations were fabricated using two different types of bilayer (TTB) thicknesses, as follows. The first TTB configuration consisted of 10 repetitions of a 10 nm Cu/3 nm W bilayer deposited on top of the buffer layer, followed by 10 repetitions of a 3 nm Cu/3 nm W bilayer (Sub + {10Cu/3W} + {3Cu/3W}). The second TTB configuration consisted of 10 repetitions of a 3 nm Cu/3 nm W bilayer on top of the buffer layer followed by 10 repetitions of a 10 nm Cu/3 nm W bilayer (Sub + {3Cu/3W} + {10Cu/3W}). In addition, NML configuration with only one type of bilayer (OTB) thickness were fabricated for comparison. One OTB configuration consisted of 20 repetitions of a 10 nm Cu/3 nm W bilayer on top of the W buffer layer (Sub + {10Cu/3W}). Moreover, a pure W thin (polycrystalline) film with a thickness of 200 nm was deposited on the α-Al_2O_3 (0 0 0 1) substrate. The NMLs with TTB, as deposited on the 500 μm thick substrates, were isothermally annealed for 100 min at various temperatures in the range of 400–800 °C under high vacuum conditions (<10^{-5} mbar), while applying a heating rate of 20 K/min. The samples, as investigated for the *in situ* stress curvature, were deposited with the same conditions listed above, on a 330 μm thick sapphire substrates.

2.2. Characterization methods

Cross-sectional cuts of the as-deposited and annealed NMLs were prepared by a Hitachi IM4000Ar ion milling system (acceleration voltage of 6 kV, discharge voltage of 1.5 kV, a swing angle of ± 30°). Planar and cross-sectional imaging was performed by scanning electron microscopy (SEM) analysis using a Hitachi S-4800 instrument.

A Bruker D8 Discover X-ray diffractometer operating in Bragg-Brentano geometry with Cu $K\alpha_{1,2}$ radiation at 40 kV/40 mA was used to measure the mean residual stress in point focus geometry. Stress analysis was carried out using the Crystallite Group Method (CGM) [41], suitable for highly textured systems (deposited Cu/W NMLs possess a pronounced in-plane and out-of-plane Cu{1 1 1} <–1 0 1>||W{1 1 0} <–1 1 1 > texture [14,28,29]). Multiple reflections belonging to the Cu <1 1 –2> and W <1 –2 1> crystallite groups were selected for stress analysis. All annealed NMLs were measured *ex situ* after cooling down to room temperature (RT).

The experimental analyses of the residual W strain depth profiles in the thin film and NMLs were performed by in-plane grazing incidence diffraction (IP-GID) using a Bruker D8 Discover diffractometer (Cu $K\alpha_{1,2}$ radiation). The diffractometer is equipped with the X-ray tube rotated, such that the diffraction vector lies parallel to the NML (film) surface, which allows to access reflections of crystallographic lattice planes that are normal to the surface (for more details about IP-GID technique see Refs. [42–44]). The in-plane diffraction scans used for the stress profile analysis contain all the W reflections perpendicular to the {1 1 0} plane. For the case of a Cu thin film with a pronounced {1 1 1} texture, only the Cu (2 2 0) reflection is assessable by in-plane diffraction. However, due to the overlapping of the Cu (2 2 0) with the W (2 1 1) reflections, the respective strain profile of Cu in the Cu/W NMLs could not be derived.

The in-plane scans were acquired at different incident angles to maximize the contribution at the different depths below the NML surface. The strain depth profiles were derived from the experimental data by an opportune modelling procedure, developed by Cancellieri et al. [45]. The strain depth profile is extracted by fitting the experimental IP-GID data with the direct Laplace transform of a generic series (power series), whose coefficients are adjusted by a least squares method. The W strain depth profiles were derived accordingly for the following configurations: as-deposited Sub + {10Cu/3W} + {3Cu/3W} NML, as-deposited and post-annealed (at 600 °C) Sub + {3Cu/3W} + {10Cu/3W} NML, as-deposited Sub + {10Cu/3W} NML, 200 nm think W thin film. Details of the fitting procedure are presented in Supplementary materials, Part I.

The sputter deposition chamber is equipped with a multi-beam optical stress sensor (MOSS) system (k-space Associates) for *in situ* measurement of the substrate curvature during thin-film growth. In this setup, a 3 × 3 array of laser beams is directed to the substrate surface under a (near-)normal incidence angle. The distance between the incident spots of the laser beams in the array was in the range of 1 mm. The real time evolution of the stress-thickness product (the force per unit width), as given by the product between the average stress and film thickness according to the well-known Stoney's equation [46], was calculated from the change in the average spacing between adjacent laser spots in the array. The MOSS system has a typical curvature resolution of about 3 × 10^{-4} m^{-1}. For more details see Refs. [47–49].

3. Graded Cu/W multilayer design

Cu/W NMLs are known to accumulate large residual in-plane compressive stresses in the Cu and W nanolayers during magnetron sputtering: the magnitude varies from ~ −2.5 GPa to ~ −0.6 GPa in Cu and from ~ −6.8 GPa to ~ −3.0 GPa in W, depending on the individual nanolayer thickness [14] and deposition conditions [38]. The total residual stress acting on each nanolayer after deposition is the result of the superposition of various types of stress contributions, such as interface stress [50], coherency stress (misfit of interplanar distances between adjacent nanolayers), deposition stress [51] and thermal stress (by the difference in thermal expansion coefficient between Cu, W and the sapphire substrate).

The interface stress f represents the work to deform a unit of pre-existed area of interface by a unit strain [50]. This implies that the Cu/W interface stress f in Cu/W NMLs deposited under identical conditions is an intrinsic property of the Cu/W interface with a specific crystallographic orientation relationship (COR); in other words, the interface stress should not depend on the Cu and W bilayer thicknesses. The relative contribution of the interface stress to the total stress in the NML system increases with decreasing bilayer thickness [50]. The interface stress for (1 1 1)Cu/(1 1 0)W interfaces (using the model developed by Ruud et al. [52]) was experimentally derived and found to be 11.25 J/m^2 (in thin films interface stress is considered as force per width N/m), which is typically presented with the J/m^2 dimension) for a COR according to Cu{1 1 1} <–1 0 1>||W{1 1 0} <–1 1 1> (as taken isotropic along the principle directions, i.e. $f_{11} = f_{22} = f$, $f_{12(21)} = 0$) [14]. This interface stress value is strikingly larger than the reported interface stress in other material systems, such as Ag/Ni (–2.27 J/m^2) [52], Ag/Cu (–3.19 J/m^2) [53] and Ag/Fe (–1.80 J/m^2) [54]. Note that a positive f value is balanced by a bulk compressive stress in the adjoined nanolayers, whereas a negative f value is compensated by a tensile stress in the adjoined nanolayers.

As shown in Refs. [14,29], the NML-to-NC transition proceeds after relaxation of the compressive stresses in the W nanolayers, which sets in at a temperature in the range of 750–900 °C. The residual stresses in the Cu nanolayers already relax at much lower temperatures in the range of 400–500 °C by diffusion creep [14,28,29]. The in-depth stress gradient across the as-deposited NML stack (from more compressive at the substrate/NML interface to less compressive towards the free NML surface) drives the directional diffusion of Cu towards the NML surface, resulting in the formation of Cu surface particles. However, as evidenced by cross-sectional imaging below such Cu surface particles [14], not all the underlying Cu nanolayers contribute to the diffusion creep process. Roughly, half of the NML structure underneath remains intact (Fig. 6 in Ref. [14]); stress relaxation in these bottom nanolayers has predominantly occurred by dislocation creep, which typically dominates at low homologous temperatures and high stress levels

[55,56]. Hence, stress relaxation in the Cu nanolayers at the onset of the NML-to-NC transformation by diffusion creep competes with dislocation creep. The Cu surface outflow kinetics will thus depend on the depth distribution of residual stresses (strains) in the as-deposited NML. For instance, a lower magnitude of residual stresses in the upper part of the NML is expected to enhance the contribution to stress relaxation by diffusion creep (as compared to the dislocation creep contribution). The respective stress (elastic strain) gradient from the bottom (more compressive) to the top (less compressive) of the NML will also be steeper, resulting in a higher driving force for directional Cu outflow. The contribution of interface stress to the total stress will be larger for thinner nanolayers [57]. Hence, the distribution of residual stresses (elastic strains) across the NML thickness can be tailored by smart variation of the bilayer thicknesses in the NML stack and studied experimentally from the Cu outflow characteristics after post-annealing. The schematic layout and cross-sectional images of the as-deposited NMLs with different bilayer thicknesses are presented in Fig. 1.

4. Results and discussion

4.1. Microstructural evolution of Cu/W NMLs upon high-temperature annealing

4.1.1. Cu outflow characteristics

As discussed in Section 3, thermal annealing activates residual stress relaxation (plastic strain increment) in the upper Cu nanolayers by diffusion creep in the form of Cu surface outflow. Fig. 2 shows representatives NML surface areas with Cu outflow after annealing of the TTB NMLs in the temperature range of 400–600 °C. For both types of investigated TTB NMLs, the shape of Cu surface crystals evolves from faceted whiskers to sphere-like particles with increasing annealing temperature, as previously reported for OTB NMLs in Ref. [14]; the size and amount of Cu surface particles also increases with increasing annealing temperature. After annealing at 400 °C, the density of Cu particles on the NML surface is nearly equal for both TTB NML types. However, after annealing at the temperatures of 500 and 600 °C, there is a dramatic increase in the amount of Cu surface particles for the Sub + {3Cu/3W} + {10Cu/3W} NML. Such a thermal activation of the Cu outflow process is typical for stress relaxation by diffusion creep. For comparison the SEM image of the surface of Sub + {10Cu/3W} NML with OTB annealed at 600 °C is presented, where it can be seen that the amount of Cu particles is sufficiently smaller. Thus, the presence of thinner 3 nm Cu/3 nm W bilayers in the bottom stack intensifies the outflow of Cu atoms from the upper 10 nm Cu/3 nm W bilayer stack. The Sub + {10Cu/3W} + {3Cu/3W} NMLs, as constituted of thicker 10 nm Cu/3 nm W bilayers in the bottom stack, show the opposite behavior. Increasing the annealing temperature to 700 °C results in the disappearance of Cu surface particles; they dissolve and diffuse back to the NML interior, as accompanied by the degradation of NML, as previously observed for OTB NMLs [14].

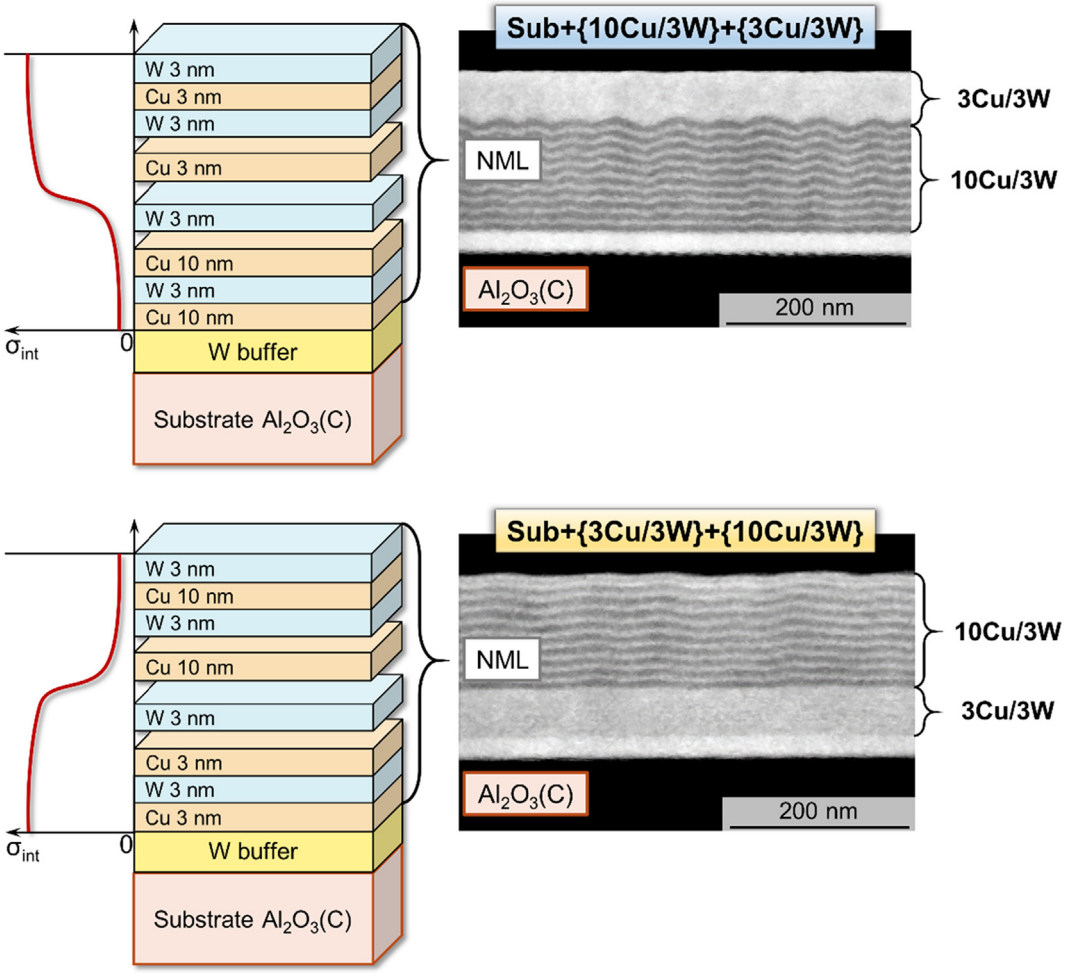

Fig. 1. Schematic representation of the investigated TTB Cu/W NMLs, also showing a representation of the expected distribution of bulk stresses as function of depth below the NML surface (as governed by the interface stress) on the left. Secondary electron micrographs of representative Cu/W NMLs are shown on the right.

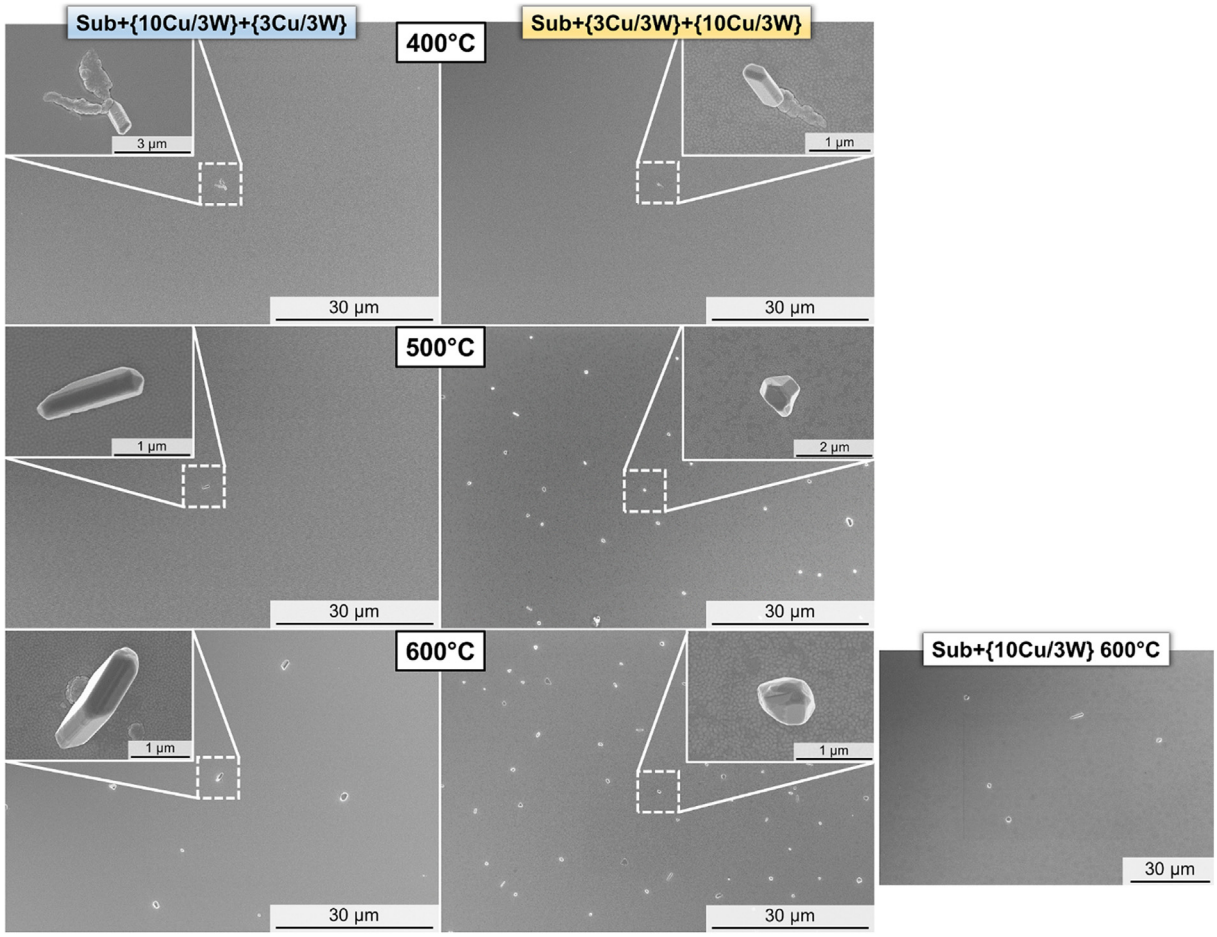

Fig. 2. SEM images of the TTB NML surfaces after thermal annealing at 400 – 600 °C and of the Sub + {10Cu/3W} NML surface after thermal annealing at 600 °C. Insets display high-magnification images of Cu surface particles to show their typical shape at each annealing temperature.

4.1.2. The NML-to-NC transition

Upon thermal treatment at $T \geq 800$ °C, both TTB NMLs undergo complete degradation of their nanolaminated structure; i.e. thermal grooving of W/W grain boundaries, pinching-off of Cu and W nanolayers and spheroidization of residual W nanolayer fragments embedded in a Cu matrix. These observations are consistent with the previously reported NML-to-NC transformation in Cu/W OTB NMLs [14,28]. Remarkably, traces of the initial microstructure of the Sub + {10Cu/3W} + {3Cu/3W} and Sub + {3Cu/3W} + {10Cu/3W} NMLs are kept during the NML-to-NC transformation: i.e. NCs with a nonuniform microstructure are formed. The cross-sectional secondary electron micrographs in Fig. 3 (lower panels) indicate that the borders between the original {3Cu/3W} and {10Cu/3W} substacks (dashed line) are preserved after the NC transformation. Hence, during the initial stage of the NML-to-NC transformation, the {3Cu/3W} and {10Cu/3W} substacks evolve independently. Undoubtedly, it is expected that much longer annealing times ($\gg$100 min) should eventually lead to a homogenization of the NC microstructure.

Both TTB NMLs interact differently with the thick W buffer layer at the bottom of the NML stack. For the Sub + {3Cu/3W} + {10Cu/3W} NML (lower panel of Fig. 3b), the buffer layer volume increases due to the inward diffusion of W atoms from the degraded 3 nm Cu/3 nm W bilayers. On the contrary, for the Sub + {10Cu/3W} + {3Cu/3W} NML, the W buffer layer is conserved, as reflected by a sharp boundary plane between the W buffer layer and the NML stack (lower panel of Fig. 3a). A similar interaction of the NML stack with the bottom W buffer layer for a 3Cu/3W OTB NML has been earlier observed: see Fig. 3a in Ref. [14].

Notably, as for the OTB NMLs [14], the formation of the NC microstructure is accompanied by the appearance of pores/voids (see inserts in upper panels in Fig. 3). Such pore formation was also revealed by Vüllers et al. [58] during the decomposition of Cu/W supersaturated solid solution films. This phenomenon can be attributed to the partial reestablishment of coherency stresses in the contacting Cu and W phases during the NML-to-NC transformation. Namely, as follows from the conventional Griffith arguments for crack nucleation and propagation [59], the creation of inner pores (i.e., of extra surface area) in the Cu/W nanocomposite can partially relax the misfit strain energy of the newly formed Cu/W interfaces. The associated overall decrease of the misfit energy compensates for the associated increase of the Cu surface energy. In particular, Zhdanov et al. in Ref. [60] proposed this as an alternative explanation for nanopore formation in oxidized metal nanoparticles (instead of the well-known Kirkendall effect).

4.2. Residual stresses in as-deposited and annealed Cu/W NMLs

4.2.1. Stress evolution during NML growth

Wafer curvature measurements by the MOSS system are typically reported as the stress-thickness product as function of the total thickness [21]. Accordingly, in Fig. 4a-c, the *in situ* stress evolution of the Cu and W nanolayers during each successive deposition step are presented as the stress-thickness product versus the total NML thickness. The stress-thickness product is directly pro-

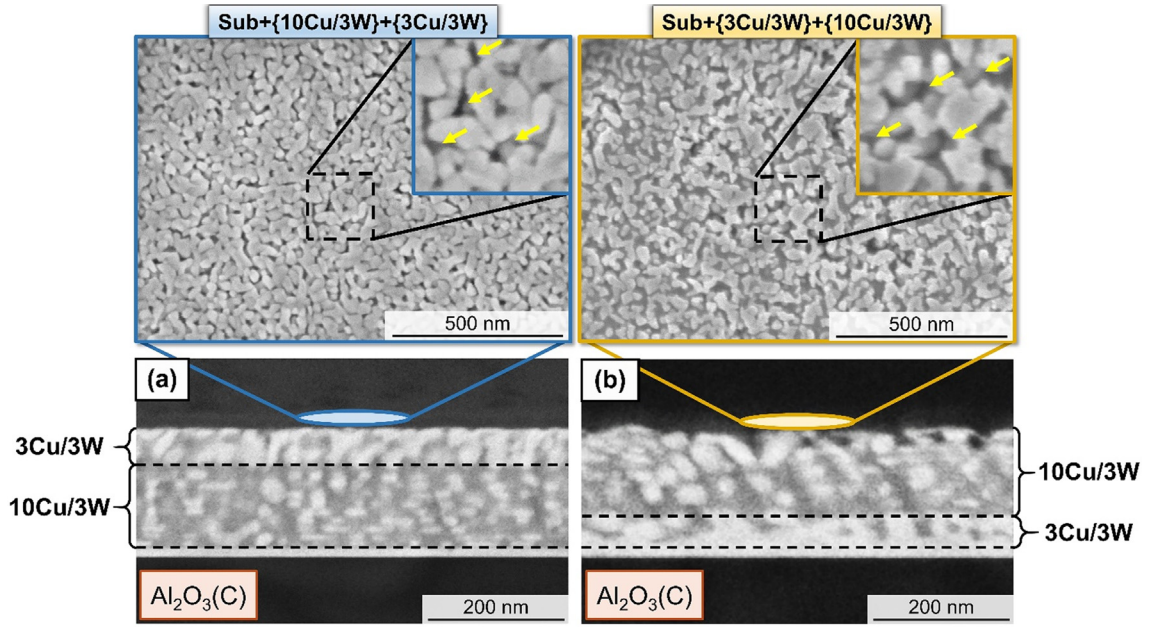

Fig. 3. SEM micrographs of cross-sections (lower panel, backscattered electron image) and respective surfaces (upper panel, secondary electron image) of the TTB Cu/W NMLs after 800 °C annealing, indicative of the NML-to-NC transition. The dashed horizontal lines in the lower panels indicate the positions of the boundary planes between the {3Cu/3W} and {10Cu/3W} bilayer substacks and the W buffer layer. Insets in upper panels are magnified images, evidencing pore/void formation in the formed NCs.

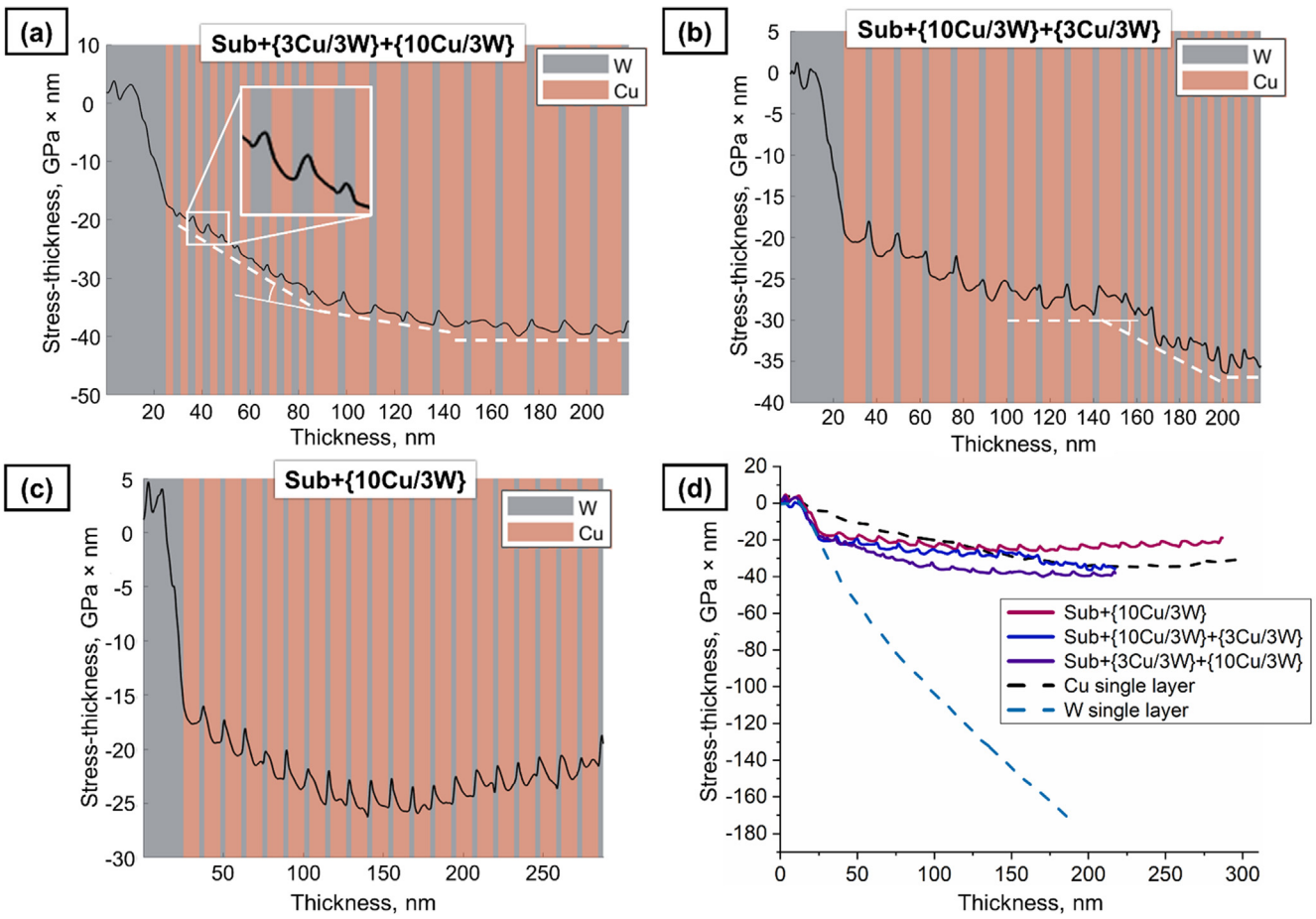

Fig. 4. The evolution of the stress-thickness product during alternating deposition steps of the Cu and W nanolayers for the Sub + {3Cu/3W} + {10Cu/3W} TTB (a), Sub + {10Cu/3W} + {3Cu/3W} TTB (b), Sub + {10Cu/3W} OTB (c) NMLs. In (d) the stress-thickness product curves of NMLs are compared with the stress-thickness product curves for Cu and W single-layer growth.

portional to the substrate curvature (through the Stoney equation [46]) in function of the NML thickness [21]. To be noted, in the inset in Fig. 4a, the peak hump during the W layer growth is clearly visible and it is the indication of Vollmer-Weber or island growth [61], associated with the grain nucleation, zipping and coarsening resulting in a compressive-tensile-compressive stress curve. There is a similarity among all the derived curves: the stress-thickness product is always negative, independent on the total NML thickness, which implies the generation of an overall compressive stress during the Cu/W NML deposition process. The similar compressive stress of Cu/W NML was obtained by substrate curvature method in Ref. [62] indicating average growth stress values in the range of −1.5 GPa to −3.2 GPa, depending on the thicknesses of nanolayers. Although the overall stress in the Cu/W NMLs is compressive, the change in the stress-thickness product during the alternating Cu and W deposition steps (further denoted as the incremental stress) differs. The deposition of the Cu nanolayers, on the one hand, is associated with the addition of a negative incremental stress (negative slope), corresponding to a compressive stress contribution. The deposition of the W nanolayers, on the other hand, results in the addition of a positive incremental stress (positive slope), implying an additive tensile stress contribution (see inset in Fig. 4a). Alternating deposition steps of the Cu and W nanolayers thus result in small oscillations of the stress-thickness curve, as indicated by the inset in Fig. 4a. The evolution of the average stress in the investigated NMLs (as derived from the stress-thickness values multiplied by thickness) is shown in Fig. S3a-c in Supplementary materials, Part II. For each grown NML, the final magnitude of the average compressive stress is relatively small (~−0.3 GPa). This implies that the growth stress in the NML, on average, decreases with increasing number of Cu/W bilayer repetitions. It can be attributed to the minor influence of the substrate constraint to dislocation slip in the newly-formed nanolayers, thereby promoting the plastic deformation to relax the major part of elastic strain in nanolayers.

For the Sub + {3Cu/3W} + {10Cu/3W} NML (Fig. 4a), the deposition of the 10 nm Cu/3 nm W bilayers on top of the 3 nm Cu/3 nm W bilayers leads to a gradual decrease of the slope of the stress-thickness curve (i.e. a decrease of the additive compressive stress contribution) towards zero; i.e. the incremental stress becomes negligible. This suggests either stress relaxation or the presence of stress (elastic strain) gradients across the NML thickness [21]. On the contrary, for the Sub + {10Cu/3W} + {3Cu/3W} NML (Fig. 4b), the change of the bilayer deposition parameters (from 10 nm Cu/3 nm W to 3 nm Cu/3 nm W) causes an initial increase of the slope of the stress-thickness curve, which levels off after ~8 deposited bilayer units (out of 10): compare white dashed lines in Fig. 4a and 4b. Strikingly, the enhanced incremental stress during deposition of the {3Cu/3W} substack results in an average compressive stress comparable to the final average compressive stress in the Sub + {3Cu/3W} + {10Cu/3W} NML (see Fig. 3Sd in Supplementary materials, Part II). This suggests that the average stress level obtained after the TTB NML deposition process does not depend on the position of 3 nm Cu/3 nm W bilayers in the NML stack, but is primarily determined by the number of 3 nm Cu/3 nm W bilayers in the substack. Important to note is that the recorded stress-thickness curves are frozen after deposition; i.e. no stress relaxation is observed after the deposition flux is stopped.

Notably, the stress-thickness product evolution of the Sub + {10Cu/3W} OTB NML (Fig. 4c) is different from the TTB NMLs. A maximum average compressive stress is reached at a total thickness of ~ 150 nm. For larger thicknesses, a tensile incremental stress contribution is found and, consequently, the average compressive stress evolves towards zero. The same trend (i.e. an incremental compressive stress with increasing thickness) is observed for the deposition of the {10Cu/3W} substack in the {Sub + {10Cu/3W} + {3Cu/3W} NML (Fig. 4b); however, subsequent deposition of the {3Cu/3W} substack induces a compressive incremental stress contribution with increasing thickness instead of a levelling off of the incremental stress. This is probably related to the larger residual stress due to interface stress for thinner layers (3 nm Cu/3 nm W) which act as a force on the bottom nanolayers. These findings nicely illustrate the possibility for tailoring accumulated growth stresses in Cu/W NMLs by controlled variation of the bilayer thicknesses.

In Fig. 4d, the stress-thickness curves of the TTB and OTB NMLs are compared with the ones obtained for single Cu and W nanolayers. Evidently, the evolution of the stress-thickness curves for the Cu/W NMLs is initially similar to that of the pure W layer, since the first stage of deposition is associated with the deposition of a 25 nm thick W buffer layer, resulting in an average compressive growth stress of ~ −1.3 GPa. However, as soon as the first Cu nanolayer deposition step is performed, the incremental compressive stress levels off and the stress-thickness curves of the TTB and OTB Cu/W NMLs become very similar to that of the Cu single layer. On the contrary, continued deposition of pure W (beyond a thickness of 25 nm) results in a further accumulation of compressive growth stresses. These results clearly indicate that the stress evolution for the deposition of the Cu/W NMLs is governed by plastic deformation in the Cu nanolayers during each successive Cu nanolayer deposition step. This can be attributed to the lower yield strength of the Cu nanolayers, so the majority of dislocation loops are formed and glide in these nanolayers rather than in the stiffer W nanolayers, relaxing the average stress in the NML. This is also consistent with the independence of the average stress on the position of 3 nm Cu/3 nm W bilayers, since the relaxation is governed solely by the total amount of Cu phase in a NML stack.

4.2.2. Mean residual stress by XRD

Fig. 5 shows the mean residual stresses in the Cu and W nanolayers for the Sub + {10Cu/3W} + {3Cu/3W} and Sub + {3Cu/3W} + {10Cu/3W} TTB NMLs in their as-deposited state, as well as after thermal treatment at different temperatures, as derived by *ex situ* XRD. In the as-deposited state, the residual compressive stresses in the W nanolayers are very similar for the Sub + {10Cu/3W} + {3Cu/3W} and Sub + {3Cu/3W} + {10Cu/3W} NMLs. The average residual compressive stress in the W nanolayers decreases with increasing annealing temperature and levels off when approaching the NML-to-NC transition temperature of about 800 °C; the behavior is similar for both types of TTB NMLs.

A different behavior is observed for the Cu nanolayers. In the as-deposited state, the Cu nanolayers in the Sub + {10Cu/3W} + {3Cu/3W} NML are a bit more compressed (~−1 GPa) as compared to the Sub + {3Cu/3W} + {10Cu/3W} NML (~−0.5 GPa). A tensile stress resides in the Cu nanolayers after the annealing at $T \geq 400$ °C. It may be assumed that the stresses in the Cu nanolayers are fully relaxed at $T \geq 400$ °C and thus a tensile residual stress is induced in the Cu nanolayers upon cooling down to room temperature (since Cu has a much larger thermal expansion coefficient as compared to W [29]). In addition, high temperature annealing enhances the coherency of the Cu/W interfaces (with a COR according to Cu{1 1 1} <−1 0 1>||W{1 1 0} <−1 1 1>), which also result in a higher residual tensile coherency stress in Cu after cooling down to room temperature. In general, residual stresses in Cu nanolayers are considerably smaller than in W nanolayers, what is also proved by the experimental results on residual stresses in Cu/W multilayers presented elsewhere Ref. [38]. Large magnitudes of compressive stresses (units of GPa) are also typical in W nanolayers [62,63].

It can be concluded that the mean values of the residual stresses in Cu and W nanolayers after cooling down from the annealing temperature to room temperature are independent on the arrange-

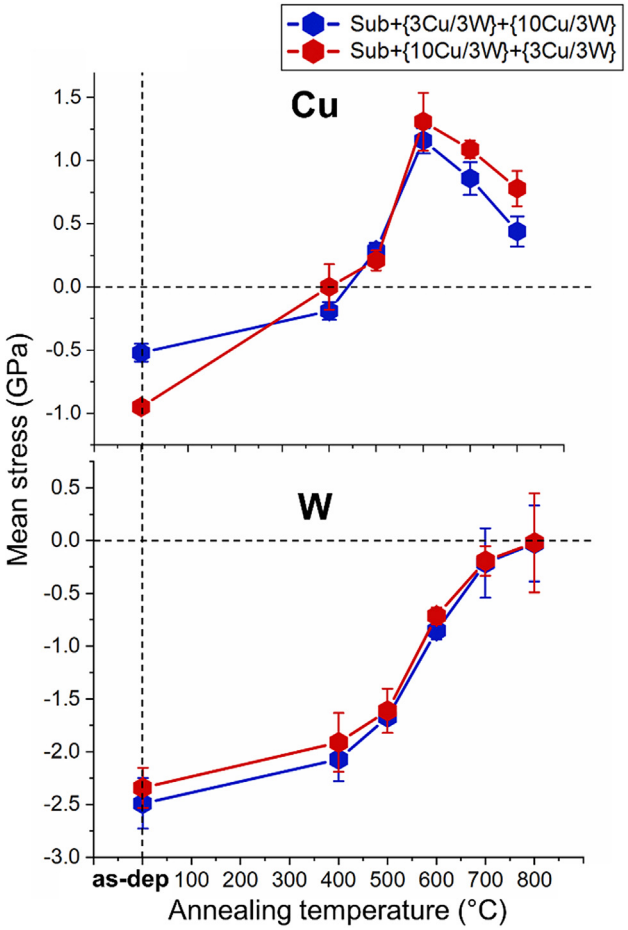

Fig. 5. Mean residual stresses in the Cu and W nanolayers for the Sub + {10Cu/3W} + {3Cu/3W} and Sub + {3Cu/3W} + {10Cu/3W} TTB NMLs, as measured *ex situ* at room temperature and as derived by the CGM model. Error bars for the mean stress values are derived from the linear fit of the lattice parameter as a function of $sin^2\,\psi$.

ment of {3Cu/3W} and {10Cu/3W} bilayer blocks in the NML volume.

4.2.3. The strain depth profiles in W nanolayers across the NML thickness

While the XRD-derived mean stresses in the W nanolayers are similar for both graded TTB Cu/W NMLs, distinct differences are found in the derived strain depth profiles. In Fig. 6a the derived W strain depth profiles are presented for the as-deposited Sub + {10Cu/3W} + {3Cu/3W}, Sub + {3Cu/3W} + {10Cu/3W} and Sub + {10Cu/3W} NMLs. The strain depth profile of the pure W thin film is shown for comparison. Unfortunately, the corresponding strain profiles of Cu could not be derived (due to the overlapping of the Cu(2 2 0) with the W(2 1 1) reflections; see Section 2). The W strain depth profiles in the NMLs and the W thin film show the largest magnitude of (compressive) strain at their interfaces with the sapphire substrate; the strain decreases with decreasing depth with respect to the outer surface. The similar profile shapes have been earlier reported in thin films, e.g. TiW [64], TiN [65]. Large values of residual stress (strain) at the substrate surface were also found in TiN/SiO_x [20], Ti/TiAlN [40] multilayers. The profile in the Sub + {3Cu/3W} + {10Cu/3W} NML resembles a slightly-curved parabolic function, whereas the profile of the Sub + {10Cu/3W} + {3Cu/3W} NML has a strongly-curved parabolic shape with a larger W strain in the NML interior (instead of at the interface). Hence, the shape of the W strain depth profile depends on the arrangement of {3Cu/3W} and {10Cu/3W} bilayer blocks in the NML volume, in contrast to the mean values of residual W stress (Fig. 5). The shapes of the strain depth profiles for the Sub + {10Cu/3W} and Sub + {10Cu/3W} + {3Cu/3W} NMLs are very similar; for the Sub + {10Cu/3W}, the W nanolayers are just more compressively strained across the NML thickness. The Sub + {10Cu/3W} + {3Cu/3W} NML can be considered as a Sub + {10Cu/3W} NML with thinner Cu nanolayers in the upper part of the NML stack.

This suggests that the *shape* of the strain depth profiles is mainly defined by the thicknesses of the Cu and W nanolayers in the bottom of the NML stack (adjacent to the NML/substrate interface), whereas the *magnitude* of the compressive strain levels is governed by the thicknesses of the Cu and W nanolayers in the rest

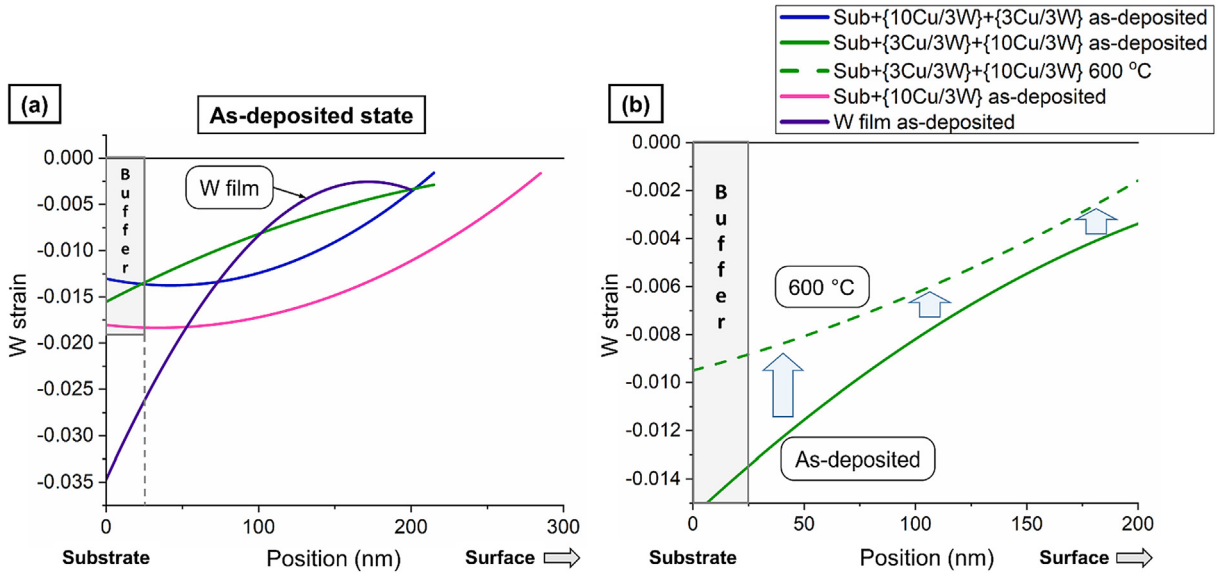

Fig. 6. The derived W strain depth profiles in the Sub + {10Cu/3W} + {3Cu/3W}, Sub + {3Cu/3W} + {10Cu/3W}, Sub + {10Cu/3W} NMLs (substrate thickness 500 μm), as well as in a pure W thin film. In (a) the strain depth profiles of the TTB and OTB NMLs, as well as of the W thin film, are presented; in (b) the strain depth profiles of the Sub + {3Cu/3W} + {10Cu/3W} TTB NML in the as-deposited state and after annealing at 600 °C (measured *ex situ*) are compared. Details of the applied method for deriving the strain depth profiles are given in the Supplementary material, Part I.

of the NML stack (i.e. adjacent to the NML surface). A possible explanation for that can be found by the impact of the substrate on the first deposited layers on the dislocation loops formation. Newly deposited layers will redistribute the elastic force also in the already formed layers underneath. This can affect the earlier formed dislocation structure (e.g. by a backward slip [66]) by changing the distribution of plastic strain across the NML thickness. This process should lead to a mechanical balance, constituting a certain shape of elastic strain distribution in nanolayers, depending on the barriers to slip in the bottom nanolayers. Moreover, important stress contribution normally occurs in the vicinity of the layer interface zone, whereas stress remains virtually constant over the coating thickness in the remainder of the curve. The contribution of higher interface stress to a measured mean value will therefore decrease continuously as the coating thickness rises. It is then clear that the shape of the strain profile depends on the thickness distribution of the nanolayers and the distances between the interfaces.

The shape of the strain depth profile in the W thin film differs from those of the TTB and OTB NMLs; the W film shows the highest rate of the strain increase, when moving from the film surface towards the substrate surface and also exhibits the largest strain of ~ 3.5% at the film/substrate interface. This difference can be attributed to the dislocation interaction in the slip systems; since in NMLs dislocation loops are dominantly gliding in individual nanolayers due to the discontinuity of the slip systems of adjacent nanolayers, in a single film dislocations can glide across the film thickness in the relevant slip planes, being constrained to slip at the film/substrate interface, thereby acting as obstacles for the newly-formed dislocations and resulting in the formation of vertical dislocation arrays. In Fig. 6b the W strain depth profile of the annealed at 600 °C Sub + {3Cu/3W} + {10Cu/3W} is compared to that of the as-deposited NML. It follows that the curvature of the profile is changed upon annealing and the profile is completely shifted to lower strain levels.

The shape of the strain depth profiles in the Sub + {10Cu/3W} + {3Cu/3W} and Sub + {3Cu/3W} + {10Cu/3W} NMLs, parabolic and near-linear respectively, can be the key to rationalize the dramatic difference of the Cu surface outflow upon annealing, as observed in Fig. 2. The Sub + {3Cu/3W} + {10Cu/3W} NML exhibits more pronounced Cu surface outflow than the Sub + {10Cu/3W} + {3Cu/3W} NML. If to assume that the shape of the strain depth profiles in Cu nanolayers are similar to those of the W nanolayers, it may be argued that the confined Cu nanolayers in the NML interior experience a higher compressive stress state for the Sub + {10Cu/3W} + {3Cu/3W} NML. This in turn would imply that the contribution to stress relaxation by dislocation creep is enhanced in the Sub + {10Cu/3W} + {3Cu/3W} NML, resulting in less pronounced Cu outflow by diffusion creep. Thus, the impact of the spatial bilayer arrangement in the NML volume on the Cu outflow intensity can be rationalized through the strain distribution in the W and Cu nanolayers across the NML thickness, supporting the idea, stated in Section 3.

5. Conclusions

The effect of a graded bilayer design on the depth distribution of strain in Cu/W NML, as well as on the mean values of the residual stresses in nanolayers, were investigated. The strain depth profiles in NMLs were for the first time experimentally accessed by an innovative experimental-modelling approach and compared to the stress measured by the substrate curvature measured during the different nanolayer deposition steps. It was found that, although the average stress level in the Cu/W NMLs does not depend on the arrangement of bilayer blocks in the NML volume, the derived shapes of depth profiles of strain in W nanolayers strongly relies on the disposition of Cu/W bilayer blocks in the NML volume. This confirms that experimental studies of the average stress state in thin films and NMLs by conventional XRD methods generally cannot disclose the true effect of residual stresses/strains i.e. stress/strain gradients on e.g. the film integrity or reactivity and that the multilayer design is paramount in tailoring the strain profile. The obtained W strain depth profile in a multilayer architecture is also unlike the one of a W single layer of similar thickness.

It was experimentally derived that the shape of strain depth profiles (the curvature of the parabolic profiles) depends on the arrangement of Cu and W nanolayers with different thicknesses across the NML depth. Thus, the strain depth distribution in Cu/W NML can be shaped by a smart design of the disposition of bilayer substacks. Moreover, upon annealing in the temperature range of 400–600 °C, Cu surface outflow was found to be dependent on the shape of strain depth profiles. Hence, the design of the bilayer blocks arrangement in the NML volume can be considered as the tool to tailor the surface outflow, as envisaged for dedicated and functionalized high-temperature joining applications [27].

The NML-to-NC (nano-multilayer-to-nanocomposite) transformation (upon annealing at 800 °C) results in an inhomogeneous NC structure, which resembles a fingerprint of the original Cu/W bilayer substacks. The proposed graded bilayer configuration of Cu/W NMLs can be thus exploited as innovative designing synthesis route in multilayer technologies for producing nanocomposites with graded bulk microstructure i.e., gradually varied mechanical, electrical and thermal properties across the NML thickness.

Data availability

The raw data required to reproduce the results of XRD in plane measurements, stress-curvature during growth and the plane spacing values used for the fitting of the strain gradient in Cu/W multilayers are available to download from 10.5281/zenodo.5084314. Important information to reproduce the presented data and the fittings are also reported in the supplementary material.

Declaration of Competing Interest

The authors declare that they have no known competing financial interests or personal relationships that could have appeared to influence the work reported in this paper.

Acknowledgement

This work was funded by the EU FP7-PEOPLE-2013-IRSES Project EXMONAN- Experimental investigation and modelling of nanoscale solid state reactions with high technological impact (Grant No. 612552); by RFBR, project number 19-33-90125; by Ministry of Education and Science of the Russian Federation in the framework of state tasks; by CSIC and PEDECIBA-FÍSICA (Uruguay) The authors would like to acknowledge the Swiss National Science Foundation (project number 200021_192224) for financially supporting this research. The Empa center for X-ray analytics is acknowledged for the support with the in-plane diffraction measurements.

Appendix A. Supplementary material

Supplementary data to this article can be found online at https://doi.org/10.1016/j.matdes.2021.110002.

References

[1] A. Sáenz-Trevizo, A.M. Hodge, Nanomaterials by design: a review of nanoscale metallic multilayers, Nanotechnology. 31 (29) (2020) 292002, https://doi.org/10.1088/1361-6528/ab803f.

[2] Z. Zhong, W. Zhan-Shan, Z. Jing-Tao, W.u. Yong-Rong, M.u. Bao-Zhong, W. Feng-Li, Q. Shu-Ji, C. Ling-Yan, Design, Fabrication and Measurement of Ni/Ti Multilayer Used for Neutron Monochromator, Chinese Phys. Lett. 24 (12) (2007) 3365–3367, https://doi.org/10.1088/0256-307X/24/12/021.

[3] T.W. Barbee Jr., Multilayers For X-Ray Optics, Opt. Eng. 25 (1986) 898–915, https://doi.org/10.1117/12.7973929.

[4] M.N. Baibich, J.M. Broto, A. Fert, F.N. Van Dau, F. Petroff, P. Etienne, G. Creuzet, A. Friederich, J. Chazelas, Giant Magnetoresistance of (001)Fe/(001)Cr Magnetic Superlattices, Phys. Rev. Lett. 61 (21) (1988) 2472–2475, https://doi.org/10.1103/PhysRevLett.61.2472.

[5] D.H. Mosca, F. Petroff, A. Fert, P.A. Schroeder, W.P. Pratt, R. Laloee, Oscillatory interlayer coupling and giant magnetoresistance in Co/Cu multilayers, J. Magn. Magn. Mater. 94 (1-2) (1991) L1–L5, https://doi.org/10.1016/0304-8853(91)90102-G.

[6] A. Misra, J.P. Hirth, R.G. Hoagland, Length-scale-dependent deformation mechanisms in incoherent metallic multilayered composites, Acta Mater. 53 (18) (2005) 4817–4824, https://doi.org/10.1016/j.actamat.2005.06.025.

[7] J. Wang, Q. Zhou, S. Shao, A. Misra, Strength and plasticity of nanolaminated materials, Mater. Res. Lett. 5 (1) (2017) 1–19, https://doi.org/10.1080/21663831.2016.1225321.

[8] A. Misra, H. Kung, Deformation Behavior of Nanostructured Metallic Multilayers, Adv. Eng. Mater. 3 (2001) 217–222, https://doi.org/10.1002/1527-2648(200104)3:4<217::AID-ADEM217>3.0.CO;2-5.

[9] C. Cancellieri, E.A. Scott, J. Braun, S.W. King, R. Oviedo, C. Jezewski, J. Richards, F. La Mattina, L.P.H. Jeurgens, P.E. Hopkins, Interface and layer periodicity effects on the thermal conductivity of copper-based nanomultilayers with tungsten, tantalum, and tantalum nitride diffusion barriers, J. Appl. Phys. 128 (19) (2020) 195302, https://doi.org/10.1063/5.0019907.

[10] X. Zhang, K. Hattar, Y. Chen, L. Shao, J. Li, C. Sun, K. Yu, N. Li, M.L. Taheri, H. Wang, J. Wang, M. Nastasi, Radiation damage in nanostructured materials, Prog. Mater. Sci. 96 (2018) 217–321, https://doi.org/10.1016/j.pmatsci.2018.03.002.

[11] J. Lipecka, J. Janczak-Rusch, M. Lewandowska, M. Andrzejczuk, G. Richter, L.P. H. Jeurgens, Thermal stability of Al-Si12at.% nano-alloys confined between AlN layers in a nanomultilayer configuration, Scr. Mater. 130 (2017) 210–213, https://doi.org/10.1016/j.scriptamat.2016.12.016.

[12] V. Araullo-Peters, C. Cancellieri, M. Chiodi, J. Janczak-Rusch, L.P.H. Jeurgens, Tailoring Fast Directional Mass Transport of Nano-Confined Ag–Cu Alloys upon Heating: Effect of the AlN Barrier Thickness, ACS Appl. Mater. Interfaces. 11 (6) (2019) 6605–6614, https://doi.org/10.1021/acsami.8b19091.

[13] M. Chiodi, C. Cancellieri, F. Moszner, M. Andrzejczuk, J. Janczak-Rusch, L.P.H. Jeurgens, Massive Ag migration through metal/ceramic nano-multilayers: an interplay between temperature, stress-relaxation and oxygen-enhanced mass transport, J. Mater. Chem. C. 4 (22) (2016) 4927–4938, https://doi.org/10.1039/C6TC01098A.

[14] A.V. Druzhinin, D. Ariosa, S. Siol, N. Ott, B.B. Straumal, J. Janczak-Rusch, L.P.H. Jeurgens, C. Cancellieri, Effect of the individual layer thickness on the transformation of Cu/W nano-multilayers into nanocomposites, Materialia. 7 (2019) 100400, https://doi.org/10.1016/j.mtla.2019.100400.

[15] L. Lin, J. Huo, G. Zou, L. Liu, L.P.H. Jeurgens, Y.N. Zhou, Maskless Patterning of Metal Outflow in Alternating Metal/Ceramic Multiple Nanolayers by Femtosecond Laser Irradiation, J. Phys. Chem. C. 124 (1) (2020) 1178–1189, https://doi.org/10.1021/acs.jpcc.9b09884.

[16] L. Lin, L.P.H. Jeurgens, Local Deformation-Controlled Fast Directional Metal Outflow in Metal/Ceramic Nanolayer Sandwiches upon Low Temperature Annealing, ACS Appl. Mater. Interfaces. 11 (42) (2019) 39046–39053, https://doi.org/10.1021/acsami.9b10498.

[17] A.C. Lewis, D. Josell, T.P. Weihs, Stability in thin film multilayers and microlaminates: the role of free energy, structure, and orientation at interfaces and grain boundaries, Scr. Mater. 48 (8) (2003) 1079–1085, https://doi.org/10.1016/S1359-6462(02)00629-2.

[18] G. Kaptay, J. Janczak-Rusch, L.P.H. Jeurgens, Melting Point Depression and Fast Diffusion in Nanostructured Brazing Fillers Confined Between Barrier Nanolayers, J. Mater. Eng. Perform. 25 (8) (2016) 3275–3284, https://doi.org/10.1007/s11665-016-2123-3.

[19] J.L. Beuth, S.H. Narayan, Residual stress-driven delamination in deposited multi-layers, Int. J. Solids Struct. 33 (1) (1996) 65–78, https://doi.org/10.1016/0020-7683(95)00021-2.

[20] J. Keckes, R. Daniel, J. Todt, J. Zalesak, B. Sartory, S. Braun, J. Gluch, M. Rosenthal, M. Burghammer, C. Mitterer, S. Niese, A. Kubec, 30 nm X-ray focusing correlates oscillatory stress, texture and structural defect gradients across multilayered TiN-SiOx thin film, Acta Mater. 144 (2018) 862–873, https://doi.org/10.1016/j.actamat.2017.11.049.

[21] G. Abadias, E. Chason, J. Keckes, M. Sebastiani, G.B. Thompson, E. Barthel, G.L. Doll, C.E. Murray, C.H. Stoessel, L. Martinu, Review Article: Stress in thin films and coatings: Current status, challenges, and prospects, J. Vac. Sci. Technol. A Vacuum, Surfaces, Film. 36 (2) (2018) 020801, https://doi.org/10.1116/1.5011790.

[22] S. Wen, R. Zong, F. Zeng, Y. Gao, F. Pan, Evaluating modulus and hardness enhancement in evaporated Cu/W multilayers, Acta Mater. 55 (1) (2007) 345–351, https://doi.org/10.1016/j.actamat.2006.07.043.

[23] L. Romano Brandt, E. Salvati, E.L. Bourhis, A.M. Korsunsky, Mode I fracture toughness determination in Cu/W nano-multilayers on polymer substrate by SEM - Digital Image Correlation, J. Mech. Phys. Solids. 145 (2020) 104145, https://doi.org/10.1016/j.jmps.2020.104145.

[24] Y. Gao, T. Yang, J. Xue, S. Yan, S. Zhou, Y. Wang, D.T.K. Kwok, P.K. Chu, Y. Zhang, Radiation tolerance of Cu/W multilayered nanocomposites, J. Nucl. Mater. 413 (1) (2011) 11–15, https://doi.org/10.1016/j.jnucmat.2011.03.030.

[25] L. Dong, H. Zhang, H. Amekura, F. Ren, A. Chettah, M. Hong, W. Qin, J. Tang, L. Hu, H. Wang, C. Jiang, Period-thickness dependent responses of Cu/W multilayered nanofilms to ions irradiation under different ion energies, J. Nucl. Mater. 497 (2017) 117–127, https://doi.org/10.1016/j.jnucmat.2017.07.064.

[26] V.V. Bukhanovsky, N.I. Grechanyuk, R.V. Minakova, I. Mamuzich, V.V. Kharchenko, N.P. Rudnitsky, Production technology, structure and properties of Cu–W layered composite condensed materials for electrical contacts, Int. J. Refract. Met. Hard Mater. 29 (5) (2011) 573–581, https://doi.org/10.1016/j.ijrmhm.2011.03.007.

[27] F. Moszner, C. Cancellieri, C. Becker, M. Chiodi, J. Janczak-Rusch, L.P.H. Jeurgens, Nano-Structured Cu/W Brazing Fillers for Advanced Joining Applications, J. Mater. Sci. Eng. B. 6 (2016) 226–230, https://doi.org/10.17265/2161-6221/2016.9-10.003.

[28] F. Moszner, C. Cancellieri, M. Chiodi, S. Yoon, D. Ariosa, J. Janczak-Rusch, L.P.H. Jeurgens, Thermal stability of Cu/W nano-multilayers, Acta Mater. 107 (2016) 345–353, https://doi.org/10.1016/j.actamat.2016.02.003.

[29] C. Cancellieri, F. Moszner, M. Chiodi, S. Yoon, J. Janczak-Rusch, L.P.H. Jeurgens, The effect of thermal treatment on the stress state and evolving microstructure of Cu/W nano-multilayers, J. Appl. Phys. 120 (19) (2016) 195107, https://doi.org/10.1063/1.4967992.

[30] L. Romano Brandt, E. Salvati, D. Wermeille, C. Papadaki, E. Le Bourhis, A.M. Korsunsky, Stress-Assisted Thermal Diffusion Barrier Breakdown in Ion Beam Deposited Cu/W Nano-Multilayers on Si Substrate Observed by in Situ GISAXS and Transmission EDX, ACS Appl, Mater. Interfaces. 13 (5) (2021) 6795–6804, https://doi.org/10.1021/acsami.0c19173.

[31] A.V. Druzhinin, C. Cancellieri, L.P.H. Jeurgens, B.B. Straumal, The effect of interface stress on the grain boundary grooving in nanomaterials: Application to the thermal degradation of Cu/W nano-multilayers, Scr. Mater. 199 (2021) 113866, https://doi.org/10.1016/j.scriptamat.2021.113866.

[32] D. Srinivasan, S. Sanyal, R. Corderman, P.R. Subramanian, Thermally stable nanomultilayer films of Cu/Mo, Metall. Mater. Trans. A. 37 (12) (2006) 995–1003, https://doi.org/10.1007/s11661-006-1019-5.

[33] D. Josell, F. Spaepen, Determination of the interfacial tension by zero creep experiments on multilayers—II. Experiment, Acta Metall. Mater. 41 (10) (1993) 3017–3027, https://doi.org/10.1016/0956-7151(93)90116-A.

[34] D. Josell, F. Spaepen, Surfaces, Interfaces, and Changing Shapes in Multilayered Films, MRS Bull. 24 (2) (1999) 39–43, https://doi.org/10.1557/S0883769400051538.

[35] M. Hecker, J. Thomas, D. Tietjen, S. Baunack, C.M. Schneider, A.n. Qiu, N. Cramer, R.E. Camley, Z. Celinski, Thermally induced modification of GMR in Co/Cu multilayers: correlation among structural, transport, and magnetic properties, J. Phys. D. Appl. Phys. 36 (5) (2003) 564–572, https://doi.org/10.1088/0022-3727/36/5/322.

[36] A. Misra, R.G. Hoagland, H. Kung, Thermal stability of self-supported nanolayered Cu/Nb films, Philos. Mag. 84 (2004) 1021–1028, https://doi.org/10.1080/14786430310001659480.

[37] H.L. Knoedler, G.E. Lucas, C.G. Levi, Morphological stability of copper-silver multilayer thin films at elevated temperatures, Metall. Mater. Trans. A. 34 (2003) 1043–1054, https://doi.org/10.1007/s11661-003-0125-x.

[38] León Romano-Brandt, Enrico Salvati, Eric Le Bourhis, Thomas Moxham, Igor P. Dolbnya, Alexander M. Korsunsky, Nano-scale residual stress depth profiling in Cu/W nano-multilayers as a function of magnetron sputtering pressure, Surf. Coatings Technol. 381 (2020) 125142, https://doi.org/10.1016/j.surfcoat.2019.125142.

[39] R. Treml, D. Kozic, J. Zechner, X. Maeder, B. Sartory, H.-P. Gänser, R. Schöngrundner, J. Michler, R. Brunner, D. Kiener, High resolution determination of local residual stress gradients in single- and multilayer thin film systems, Acta Mater. 103 (2016) 616–623, https://doi.org/10.1016/j.actamat.2015.10.044.

[40] U. Selvadurai, W. Tillmann, G. Fischer, T. Sprute, The Influence of Multilayer Design on Residual Stress Gradients in Ti/TiAlN Systems, Mater. Sci. Forum. 768–769 (2013) 264–271, https://doi.org/10.4028/www.scientific.net/MSF.768-769.264.

[41] B.M. Clemens, J.A. Bain, Stress Determination in Textured Thin Films Using X-Ray Diffraction, MRS Bull. 17 (7) (1992) 46–51, https://doi.org/10.1557/S0883769400041658.

[42] Markus Neuschitzer, Armin Moser, Alfred Neuhold, Johanna Kraxner, Barbara Stadlober, Martin Oehzelt, Ingo Salzmann, Roland Resel, Jiří Novák, Grazing-incidence in-plane X-ray diffraction on ultra-thin organic films using standard laboratory equipment, J. Appl. Crystallogr. 45 (2) (2012) 367–370, https://doi.org/10.1107/S0021889812000908.

[43] B.K. Tanner, T.P.A. Hase, T.A. Lafford, M.S. Goorsky, Grazing incidence in-plane X-ray diffraction in the laboratory, Powder Diffr. 19 (2004) 45–48, https://doi.org/10.1154/1.1649319.

[44] Kazuhiko Omote, High resolution grazing-incidence in-plane x-ray diffraction for measuring the strain of a Si thin layer, J. Phys. Condens. Matter. 22 (47) (2010) 474004, https://doi.org/10.1088/0953-8984/22/47/474004.
[45] Claudia Cancellieri, Daniel Ariosa, Aleksandr V. Druzhinin, Yeliz Unutulmazsoy, Antonia Neels, Lars P.H. Jeurgens, Strain depth profiles in thin films extracted from in-plane X-ray diffraction, J. Appl. Crystallogr. 54 (1) (2021) 87–98, https://doi.org/10.1107/S1600576720014843.
[46] G.G. Stoney, The tension of metallic films deposited by electrolysis, Proc. R. Soc. London. Ser. A, Contain. Pap. A Math. Phys. Character. 82 (1909) 172–175, https://doi.org/10.1098/rspa.1909.0021.
[47] Elisa Gilardi, Aline Fluri, Thomas Lippert, Daniele Pergolesi, Real-time monitoring of stress evolution during thin film growth by in situ substrate curvature measurement, J. Appl. Phys. 125 (8) (2019) 082513, https://doi.org/10.1063/1.5054092.
[48] E. Chason, B.W. Sheldon, Monitoring Stress in Thin Films During Processing, Surf. Eng. 19 (2003) 387–391, https://doi.org/10.1179/026708403225010118.
[49] G. Abadias, Ph. Guerin, In situ stress evolution during magnetron sputtering of transition metal nitride thin films, Appl. Phys. Lett. 93 (11) (2008) 111908, https://doi.org/10.1063/1.2985814.
[50] Robert C. Cammarata, Surface and interface stress effects in thin films, Prog. Surf. Sci. 46 (1) (1994) 1–38, https://doi.org/10.1016/0079-6816(94)90005-1.
[51] E. Chason, A kinetic analysis of residual stress evolution in polycrystalline thin films, Thin Solid Films. 526 (2012) 1–14, https://doi.org/10.1016/j.tsf.2012.11.001.
[52] J.A. Ruud, A. Witvrouw, F. Spaepen, Bulk and interface stresses in silver-nickel multilayered thin films, J. Appl. Phys. 74 (1993) 2517–2523, https://doi.org/10.1063/1.354692.
[53] S. Berger, F. Spaepen, The Ag/Cu interface stress, Nanostructured Mater. 6 (1-4) (1995) 201–204, https://doi.org/10.1016/0965-9773(95)00043-7.
[54] M.R. Scanlon, R.C. Cammarata, D.J. Keavney, J.W. Freeland, J.C. Walker, C. Hayzelden, Elastic and hardness properties of Fe–Ag (001) multilayered thin films, Appl. Phys. Lett. 66 (1995) 46–48, https://doi.org/10.1063/1.114177.
[55] M.E. Kassner, M.T. Pérez-Prado, Fundamentals of Creep in Metals and Alloys (2004), https://doi.org/10.1016/B978-0-08-043637-1.X5000-5.
[56] S. Saha, M. Motalab, Nature of creep deformation in nanocrystalline Tungsten, Comput. Mater. Sci. 149 (2018) 360–372, https://doi.org/10.1016/j.commatsci.2018.03.040.
[57] F.H. Streitz, R.C. Cammarata, K. Sieradzki, Surface-stress effects on elastic properties. I. Thin metal films, Phys. Rev. B. 49 (1994) 10699–10706, https://doi.org/10.1103/PhysRevB.49.10699.
[58] F.T.N. Vüllers, R. Spolenak, From solid solutions to fully phase separated interpenetrating networks in sputter deposited "immiscible" W-Cu thin films, Acta Mater. 99 (2015) 213–227, https://doi.org/10.1016/j.actamat.2015.07.050.
[59] T.L. Anderson, Fracture Mechanics: Fundamentals and Applications, Fourth Edition (2017).
[60] Vladimir P. Zhdanov, Bengt Kasemo, On the Feasibility of Strain-Induced Formation of Hollows during Hydriding or Oxidation of Metal Nanoparticles, Nano Lett. 9 (5) (2009) 2172–2176, https://doi.org/10.1021/nl9008293.
[61] J.A. Floro, S.J. Hearne, J.A. Hunter, P. Kotula, E. Chason, S.C. Seel, C.V. Thompson, The dynamic competition between stress generation and relaxation mechanisms during coalescence of Volmer-Weber thin films, J. Appl. Phys. 89 (2001) 4886–4897, https://doi.org/10.1063/1.1352563.
[62] B. Girault, P. Villain, E. Le Bourhis, P. Goudeau, P.-O. Renault, X-ray diffraction analysis of the structure and residual stresses of W/Cu multilayers, Surf. Coatings Technol. 201 (7) (2006) 4372–4376, https://doi.org/10.1016/j.surfcoat.2006.08.034.
[63] P. Goudeau, K.F. Badawi, A. Naudon, G. Gladyszewski, Determination of the residual stress tensor in Cu/W multilayers by x-ray diffraction, Appl. Phys. Lett. 62 (1993) 246–248, https://doi.org/10.1063/1.108979.
[64] F. Saghaeian, J. Keckes, S. Woehlert, M. Rosenthal, M. Reisinger, J. Todt, Microstructure and stress gradients in TiW thin films characterized by 40 nm X-ray diffraction and transmission electron microscopy, Thin Solid Films. 691 (2019), https://doi.org/10.1016/j.tsf.2019.137576 137576.
[65] R. Daniel, E. Jäger, J. Todt, B. Sartory, C. Mitterer, J. Keckes, Mono-textured nanocrystalline thin films with pronounced stress-gradients: On the role of grain boundaries in the stress evolution, J. Appl. Phys. 115 (20) (2014) 203507, https://doi.org/10.1063/1.4879243.
[66] Nan Li, Jian Wang, Amit Misra, Jian Yu Huang, Direct Observations of Confined Layer Slip in Cu/Nb Multilayers, Microsc. Microanal. 18 (5) (2012) 1155–1162, https://doi.org/10.1017/S143192761200133X.